Geometric nonlinear analyses of functionally graded beams using a tailored Lagrangian formulation

Carlos A. Almeida [a,*], Juan C.R. Albino [a], Ivan F.M. Menezes [b], Glaucio H. Paulino [c,d]

[a] *Mechanical Engineering, Pontifical Catholic University of Rio de Janeiro, RJ 22453-900, Brazil*
[b] *Tecgraf (Computer Graphics Technology Group), Pontifical Catholic University of Rio de Janeiro, RJ 22453-900, Brazil*
[c] *Civil & Environmental Engineering, University of Illinois at Urbana-Champaign, IL 61801-2352, USA*
[d] *National Science Foundation, 4201 Wilson Boulevard, Suite 545, Arlington, VA 22230-0002, USA*

ARTICLE INFO

ABSTRACT

This paper presents a geometric nonlinear analysis formulation for beams of functionally graded cross-sections by means of a Total Lagrangian formulation. The influence of material gradation on the numerical response is investigated in detail. Two examples are given that illustrate the main features of the formulation, in which the behavior of beams of graded cross-sections is compared with homogeneous material beams. A motivation for this work is the potential development of functionally graded risers for the offshore oil exploration industry.

© 2011 Elsevier Ltd. All rights reserved.

1. Introduction

Functionally graded materials (FGMs) possess spatially varied microstructures caused by the non-uniform distribution of the reinforcement phase and by interchanging reinforcement and matrix material roles in a continuous manner (see, for example, Yin et al., 2004; Paulino et al., 2006; Shen et al., 2008; Paulino et al., 2009). These materials have been used in several engineering applications including thermal barrier coatings and thermal protection systems, crack propagation inhibitors in multi-layer components or buckling failure prevention in thin walled members. Applications can also be observed in biomechanics (e.g. bone and dental implants), piezoelectric devices, spaceflight structures, engines, pressure vessels, and pipes. The field has rapidly advanced in several fronts including modeling, synthesis, and experiments (Suresh et al., 1993; Suresh and Mortensen, 1998; Miyamoto et al., 1999; Paulino and Sutradhar, 2006; Chen et al., 2008; Almeida et al., 2010; Choi and Paulino, 2010). This paper contributes toward numerical modeling of FGM structures and concentrates on the geometrically nonlinear behavior of functionally graded beams. We hope that the work will impart knowledge to the development and evaluation of combined materials and structural systems. In fact, a relevant application is related to the potential development of functionally graded risers, which has widespread in the petroleum industry.

Modeling of FGMs has employed a variety of techniques, including the finite element method. Most of the work has concentrated on the use of continuum element formulations (Kim and Paulino, 2002; Dave et al., 2011). However, there has been significant work using discrete elements such as plates and shells (Tutuncu, 2007; Ng et al., 2000; Reddy and Cheng, 2001). There has also been some work on beams modeled with continuum elements (Chakraborty et al., 2003; Zhang and Paulino, 2007) and with one dimension (line) elements, as in (Chakraborty et al., 2003), where a first-order shear deformation theory is employed for linear analysis of beams in statics as well as in dynamics (Reddy, 1997). This paper emphasizes on line elements in large displacement analysis, but small strains, in which the material properties vary gradually through the thickness. The through-thickness property variation plays a role in the beam behavior, which is demonstrated by comparing stress profiles of homogeneous beams with those of graded beams.

The remainder of this paper is organized as follows. Initially, Section 2 presents a brief introduction to the finite element formulation used herein. The FGM capabilities are incorporated into the finite element model in Section 3. Next, in order to assess the effectiveness of the proposed formulation, two numerical examples are presented in Section 4. Finally, conclusions are drawn, and directions for future research are pointed out in Section 5.

2. Finite element formulation review

The finite element formulation adopted in this work follows the *Total Lagrangian* approach for two-dimensional beam problems, as presented by Pacoste and Eriksson (1997). It considers the center

---

* Corresponding author. Tel.: +55 21 35271169; fax: +55 21 35271165.
  E-mail address: calmeida@puc-rio.br (C.A. Almeida).
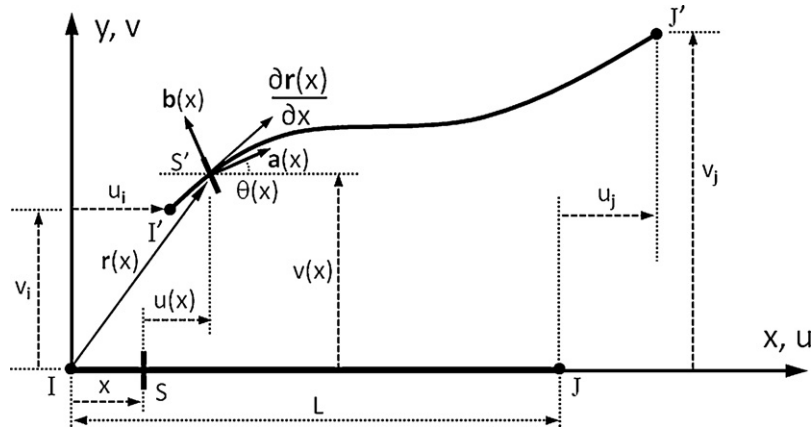
Fig. 1. Initial and deformed configurations of beam center line.

line I-J of a beam element of length L, initially straight, laying on the local x axis of a reference configuration system and undergoing to a space deformed configuration I′ − J′, as illustrated by Fig. 1. The present model takes into account kinematics for large displacements and rotations, but with small strains and shear deformations.

The beam center line I′–J′, in deformed configuration, can be described by means of position vector $\mathbf{r}(x)$, defined as (Lages et al., 1999)

$$\mathbf{r}(x) = [x + u(x)]\mathbf{i} + v(x)\mathbf{j} \tag{1}$$

where $u(x)$ and $v(x)$ are, respectively, axial and transversal displacements of a point on the beam center line axis at coordinate x and $\mathbf{i}$ and $\mathbf{j}$ are unit vectors at fixed axes x and y. Moreover, as shown in Fig. 1, this point is associated to a cross section S that may undergo large displacements and rotation to spatial position S′, according to the parameters $u(x)$, $v(x)$ and $\theta(x)$. The tangent to the beam center line I′–J′, vector $\partial\mathbf{r}(x)/\partial x$, can be expressed in terms of the beam deformation measures $\epsilon(x)$, $\gamma(x)$ and $\kappa(x)$ as

$$\frac{\partial\mathbf{r}(x)}{\partial x} = [1 + \epsilon(x)]\mathbf{a} + \gamma(x)\mathbf{b}, \qquad \kappa(x) = \frac{\partial\theta(x)}{\partial x} \tag{2}$$

where unit vectors $\mathbf{a}$ and $\mathbf{b}$ are orthogonal and parallel to the cross section S′, respectively, and can be expressed as

$$\mathbf{a}(x) = \cos\theta(x)\mathbf{i} + \sin\theta(x)\mathbf{j}, \qquad \mathbf{b}(x) = -\sin\theta(x)\mathbf{i} + \cos\theta(x)\mathbf{j} \tag{3}$$

From Eqs. (1) and (2), these deformations result, in terms of the beam displacements, as follows

$$
\begin{aligned}
\epsilon(x) &= \left[1 + \frac{\partial u(x)}{\partial x}\right]\cos\theta(x) + \left[\frac{\partial v(x)}{\partial x}\right]\sin\theta(x) - 1 \\
\gamma(x) &= -\left[1 + \frac{\partial u(x)}{\partial x}\right]\sin\theta(x) + \left[\frac{\partial v(x)}{\partial x}\right]\cos\theta(x) \\
\kappa(x) &= \frac{\partial\theta(x)}{\partial x}
\end{aligned}
\tag{4}
$$

These equations reduce to the classic Timoshenko's beam formulas if the condition of small rotation angle $\theta(x)$ is enforced, i.e. $\cos(x) \approx 1$ and $\sin(x) \approx 0$, and by neglecting the remaining second order terms. Moreover, Euler–Bernoulli deformation measures are then obtained if on top of these, pure bending identity condition is applied ($\theta(x) = dv(x)/dx$).

According to Fig. 2, N and T are, respectively, normal and transverse components of the internal force $\mathbf{F}$ acting on a generic section

S′, and M is the bending moment. In vector form, they are expressed as

$$\mathbf{F} = N\mathbf{a} + T\mathbf{b}, \qquad \mathbf{M} = M\mathbf{a} \times \mathbf{b} \tag{5}$$

where "×" denotes vector cross product operation. Imposing the equilibrium conditions on the resulting stresses and assuming a linear constitutive relation of an homogeneous material one can write

$$N = \left(\int_A E\,dA\right)\epsilon = EA\epsilon, \quad T = \left(\int_A G\,dA\right)\gamma = GA\gamma,$$

$$M = \left(\int_A Ey^2\,dA\right)\kappa = EI_z\kappa \tag{6}$$

where EA, GA and EI_z are the resulting beam cross sectional axial, shear and flexural rigidities, respectively. As shown in the next section, material gradation is incorporated into the formulation in the evaluation of these cross-sectional properties. The element strain energy U is given as

$$U = \frac{1}{2}\int_0^L \left(EA\epsilon^2 + GA\gamma^2 + EI_z\kappa^2\right)\,dx \tag{7}$$

where $\epsilon(x)$, $\gamma(x)$ and $\kappa(x)$ are as defined in Eq. (4). To avoid locking, the integral in Eq. (7) is numerically evaluated using one-point Gaussian quadrature at the element mid-point (Pacoste and Eriksson, 1997). Also, the element displacement fields $u(x)$, $v(x)$ and $\theta(x)$ are linearly interpolated along the length with respect to nodal
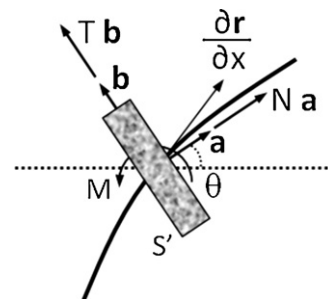
Fig. 2. Internal forces and bending moment on a beam cross section.
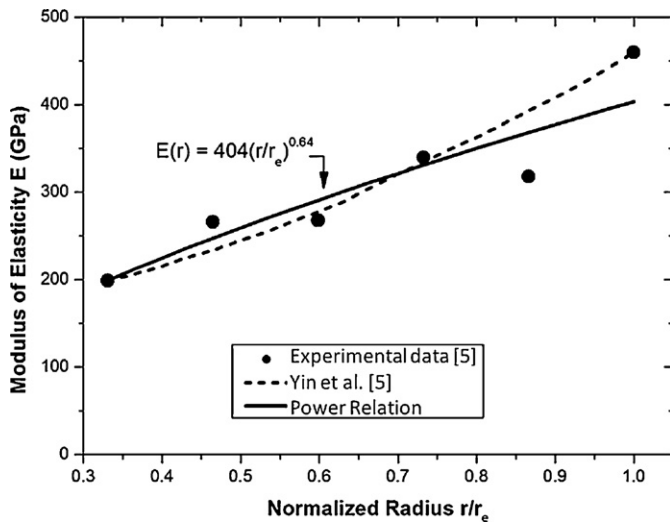
Fig. 3. Young's modulus distribution over pipe cross section thickness.

degrees of freedom $\mathbf{u}_e = \{u_I, v_I, \theta_I, u_J, v_J, \theta_J\}$. Once the interpolation functions and the integration strategy are defined, one can use

$$
\frac{\partial u(x)}{\partial x} = \frac{(u_J - u_I)}{L} \quad , \quad \frac{\partial v(x)}{\partial x} = \frac{(v_J - v_I)}{L}
$$
$$
\frac{\partial \theta(x)}{\partial x} = \frac{(\theta_J - \theta_I)}{L} \quad , \quad \theta(x) = \theta_I \left(1 - \frac{x}{L}\right) + \theta_J \left(\frac{x}{L}\right)
\tag{8}
$$

to evaluate Eq. (7). The components of the element internal force vector $\mathbf{f}_e = \{N_I, T_I, M_I, N_J, T_J, M_J\}$ and tangent stiffness matrix $\mathbf{K}_e$ are obtained by successive differentiation of U with respect to vector $\mathbf{u}_e$ components (Pacoste and Eriksson, 1997), in the form

$$
f_{e_i} = \frac{\partial U}{\partial u_{e_i}}, \qquad K_{e_{ij}} = \frac{\partial^2 U}{\partial u_{e_i} \partial u_{e_j}} \quad i,j = 1 \dots 6
\tag{9}
$$

3. FGM capabilities

This section describes the approach employed to consider functionally graded cross-section beams into the total Lagrangian formulation presented in the previous section. As an example, we consider experimental data and numerical simulation results for the Young's modulus $E(x)$ and Poisson's ratio $\nu(x)$, from a plate of TiC–Ni_3Al alloy (Yin et al., 2004), which are adjusted through thickness of a pipe cross section by means of a representation curve obtained using least square data reduction, as illustrated by Fig. 3.

In this case, a power law approximation for the distribution of E through the pipe wall is obtained as

$$
E(r) = E_e \left(\frac{r}{r_e}\right)^m
\tag{10}
$$

where E_e and m are adjusting parameters and r_e is the external radius of the pipe. The power relation shown in Eq. (10) enables one to proceed with the beam analysis using *equivalent* rigidity moduli (*e.g.*, $\overline{EA}$, $\overline{GJ}$ and $\overline{EI_z}$), all obtained in closed form in Eq. (6) from integrals over the beam cross section area, in the finite element strain energy expression (Eq. (7)). This is a general approach, suitable to any distribution provided, as shown in the examples that follow. Notice that material property variation, through the thickness of the beam, is considered in the numerical formulation, and the fact that we refer to equivalent moduli does not reduce it to an homogeneous beam. The through-thickness material property variation plays a role in the beam response, specially on the stress distributions, as shown in the next section.

4. Numerical examples

In order to illustrate the main features of the present formulation two examples are considered. The objective is to evaluate the behavior of beams of graded material through the cross-sections by comparing the results with those of homogeneous materials. In the analyses that follow both linear and geometric nonlinear behaviors of in-plane bending beams are investigated.

4.1. Bi-material FGM beam

This example, which has been considered by Chakraborty et al. (2003) and Zhang and Paulino (2007), consists of a cantilever beam subjected to a transverse tip load. As shown in Fig. 4, the beam possesses a composite cross-section made of two basic materials (Steel and Alumina) that receives a thin FGM layer between them allowing for a smooth material property transition. The numerical input data, including dimensions and all material properties, is also presented in the figure. The FGM material property is assumed to vary according to the following exponential relation

$$
E(z^*) = E_s \exp\left[\left(\frac{z^*}{a_2} - \frac{1}{2}\right) \ln\left(\frac{E_s}{E_a}\right)\right] = A.B^{(z^*/a_2)}
\tag{11}
$$

where $z^* \in \left[-a_2/2, a_2/2\right]$, $A = E_s \left(E_s/E_a\right)^{-1/2}$ and $B = E_s/E_a$.

The beam reference axis position (neutral axis), from the mid-coordinate of FGM layer, is obtained by imposing the equilibrium condition

$$
N = 0 \quad \Rightarrow \quad \int_A \sigma_x \, dA = \int_A E(z)\kappa z \, dA = 0
$$
$$
\Rightarrow \quad \int_z E(z) z \, dz = 0.
\tag{12}
$$

According to Fig. 5, and considering $z^* = z - z_1$ in Eq. (11), Eq. (12) results in the following

$$
\int_{-(a_3+(a_2/2)-z_1)}^{(z_1-(a_2/2))} E_a z \, dz + \int_{(z_1-(a_2/2))}^{(z_1+(a_2/2))} AB^{(z-z_1)/a_2} z \, dz
$$
$$
+ \int_{(z_1+(a_2/2))}^{(z_1+(a_2/2)+a_1)} E_s z \, dz = 0
\tag{13}
$$

which leads to $z_1 = 0.0128$ m.

4.1.1. Equivalent structural rigidities

Using Eqs. (6) and the numerical data in Fig. 4, equivalent structural rigidities are obtained with the material gradation law being integrated along the cross-section area of the beam shown in Fig. 5. Notice that the exponential distribution used for $E(z^*)$ in Eq. (11) is also employed for $G(z^*)$, with $z^* = z - z_1$.

4.1.1.1. (a) Axial rigidity ($\overline{EA}$).

$$
\overline{EA} = E_s A_s + \int_{(z_1-(a_2/2))}^{(z_1+(a_2/2))} AB^{(z-z_1)/a_2} b \, dz + E_a A_a = 16.754 \times 10^9 \text{ N}
\tag{14}
$$

where $A_s = b a_1$ and $A_a = b a_3$.

4.1.1.2. (b) Shear rigidity ($\overline{GA}$).

$$
\overline{GA} = G_s A_s + \int_{(z_1-(a_2/2))}^{(z_1+(a_2/2))} A'B'^{(z-z_1)/a_2} b \, dz + G_a A_a = 5.982 \times 10^9 \text{ N}
\tag{15}
$$

where $A' = G_s \left(G_s/G_a\right)^{-1/2}$ and $B' = G_s/G_a$.
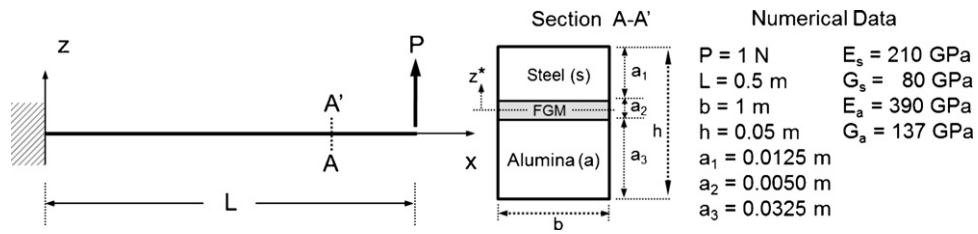
Fig. 4. The cantilever composite cross-section beam considered.
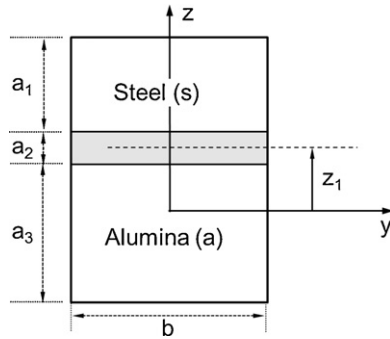
Fig. 5. Neutral axis position at composite beam cross-section.

Table 1
Analytical results for the composite cross-section beam.

Stress Component	Expression	Limits
σ_{xx} (Alumina)	$-E_a[PLz/\overline{EI}_y]$	$-0.0222 < z < 0.0103$
σ_{xx} (FGM)	$-E_{FGM}(z^*)[PLz/\overline{EI}_y]$	$0.0103 < z < 0.0153$
σ_{xx} (Steel)	$-E_s[PLz/\overline{EI}_y]$	$0.0153 < z < 0.0278$
σ_{xz} (Alumina)	$G_a[P/\overline{GA}]$	$-0.0222 < z < 0.0103$
σ_{xz} (FGM)	$G_{FGM}(z^*)[P/\overline{GA}]$	$0.0103 < z < 0.0153$
σ_{xz} (Steel)	$G_s[P/\overline{GA}]$	$0.0153 < z < 0.0278$

According to Eqs. (11)–(13) $z^* = z - z_1$, where $z_1 = 0.0128m$.

4.1.2. Numerical results

From the results in Eqs. (11)–(16), the usual FE procedure is carried out to obtain the beam nodal displacements using definitions in Eq. (9). These results are then employed to obtain the beam deformations, as defined in Eqs. (4), and correspondent stress components. Closed forms for these axial and shear stress components, at the fixed cross-section of the beam considered, are obtained according to expressions shown in Table 1. Fig. 6 illustrates these stress distributions as they are compared to obtained numerical values using a single element model and a very good agreement in the results is observed. Also, solutions for a full FGM cross section beam model are included in these comparisons. Notice that for the applied load and the geometric and material parameters consid-

4.1.1.3. (c) Flexural rigidity ($\overline{EI}_y$).

$$\overline{EI}_y = E_s I_s + \int_{(z_1-(a_2/2))}^{(z_1+(a_2/2))} AB^{(z-z_1)/a_2} z^2 b\, dz + E_a I_a = 3.044 \times 10^6\, \text{N}\,\text{m}^2 \tag{16}$$

where $I_s = ba_1^3/12 + A_s d_s^2$ and $I_a = ba_3^3/12 + A_a d_a^2$, with $d_s = z_1 + (a_1 + a_2)/2$ and $d_a = (a_2 + a_3)/2 - z_1$, respectively.
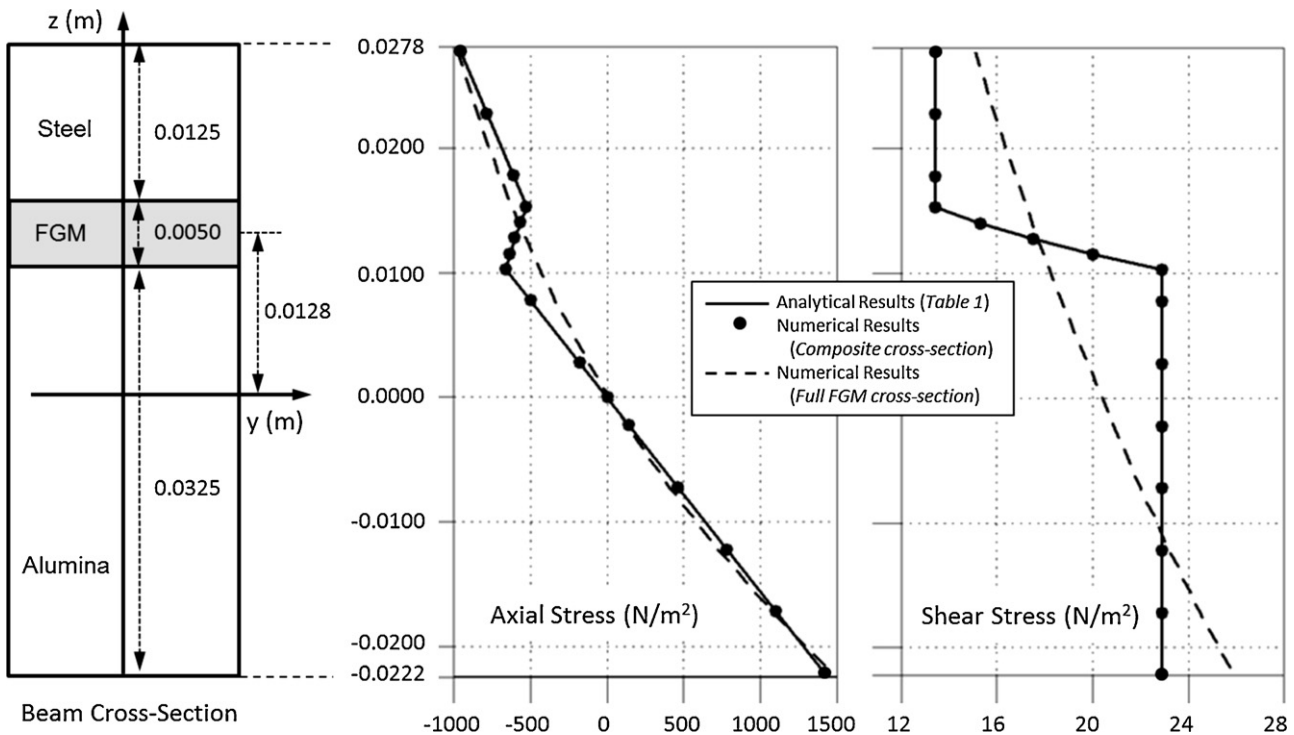
Fig. 6. Axial and shear stresses through the beam thickness at fixed end cross-section.
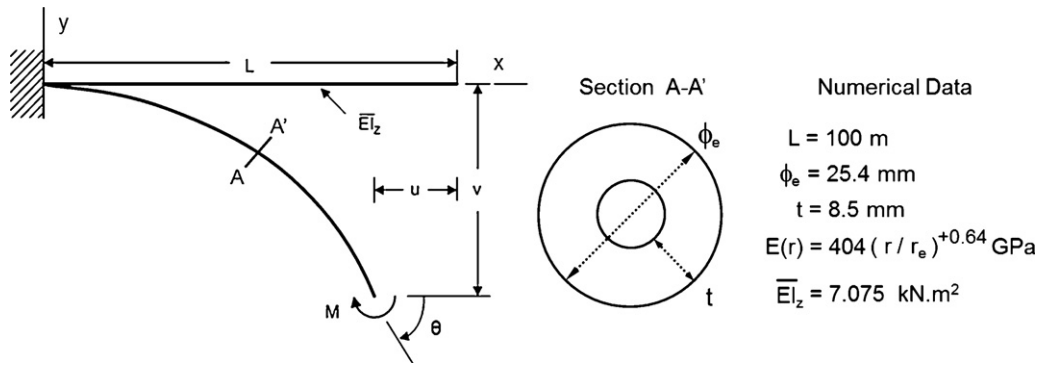
Fig. 7. Cantilever beam considered in large displacement analysis.

ered in this study, the beam response is in its linear range, although full geometric nonlinear formulation capabilities are employed. The numerical analysis responses were obtained in one load step, with no iteration requirements.

4.2. Straight cantilever beam under constant bending

Fig. 7 illustrates an initially straight pipe cross section cantilever beam subject to constant bending moment in large displacement analysis. This example reproduces a classical solid mechanics problem for which analytical solutions are compared to the obtained numerical results of a FGM beam. In the present study, geometric nonlinearities are taken into account. The numerical input data used, including beam dimensions and material property parameters, is also presented in Fig. 7. The material Young's modulus distribution through the pipe wall thickness is as in Fig. 3, having TiC and Ni_3Al at the external radius and inner radius, respectively. However, it should be noticed that this material configuration used is for simulation purposes only and may not refer to the material of a real system.

Because under constant bending the beam centerline undergoes a constant curvature configuration κ, then the tip cross-section rotation angle θ, in Fig. 7, may be obtained by analytical means using

$$\theta = \kappa L = \frac{ML}{\overline{EI_z}} \quad \text{or} \quad \theta = 2\pi\left(\frac{M}{M^*}\right) \tag{17}$$

where M^* is the required bending moment for $\theta = 2\pi$ rad, as shown in Fig. 8. From geometric considerations, the beam tip displacements are readily obtained as

$$u = L - R\sin\theta \quad \text{and} \quad v = R - R\cos\theta \tag{18}$$

where $R = 1/\kappa = L/\theta$. Thus, Eq. (18) are equivalent to

$$\frac{u}{L} = \left(1 - \frac{\sin\theta}{\theta}\right) \quad \text{and} \quad \frac{v}{L} = \frac{(1-\cos\theta)}{\theta}. \tag{19}$$

Results from the analytical expressions in Eqs. (17) and (19) are presented in Fig. 9, for $0 \le M/M^* \le 1$, which are used to evaluate the numerical responses of the cantilever beam model considered in this study.

4.2.1. Numerical results

In this analysis, 10 equally spaced elements are employed. The beam static configurations for different values of the applied end moment are shown in Fig. 8, in a qualitative manner. Measurements of horizontal and vertical displacements as well the rotations at the tip of the beam, for increasing values of the applied moment, are compared with good agreement to the analytical results, in Fig. 9. These numerical results were obtained with 100 equally incremented load steps, using Newton–Raphson iteration procedure with displacement increment tolerance of 10^{-4}. In all load steps numerical solution convergence was reached, at maximum, after four equilibrium iterations.

Finally, results for normal stress distributions in the pipe-beam section for $M = 0.6M^*$ – which corresponds to a fairly large displacement configuration, as shown in Fig. 8 – are considered. These longitudinal stresses were analytically evaluated using the expression

$$\sigma_{xx} = E(r)\epsilon_{rr} = E(r)\left(\frac{My}{\overline{EI_z}}\right) = E(r)2\pi\left(\frac{M}{M^*}\right)\left(\frac{y}{L}\right). \tag{20}$$

Fig. 8. Static equilibrium configurations for various bending loads.
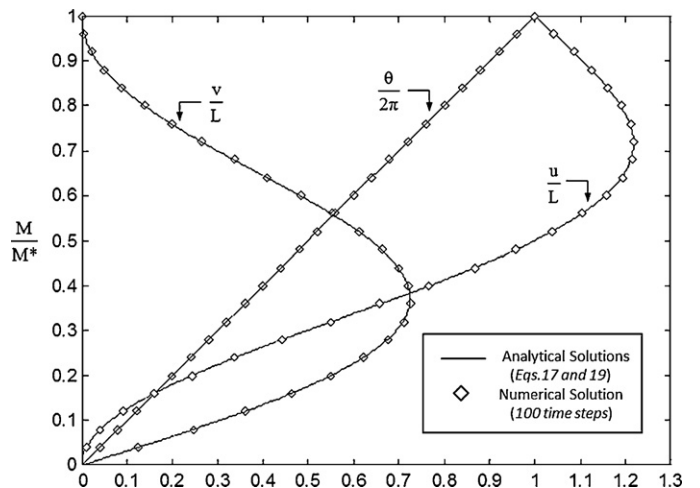
Fig. 9. Tip displacements and rotations of cantilever beam under constant bending.
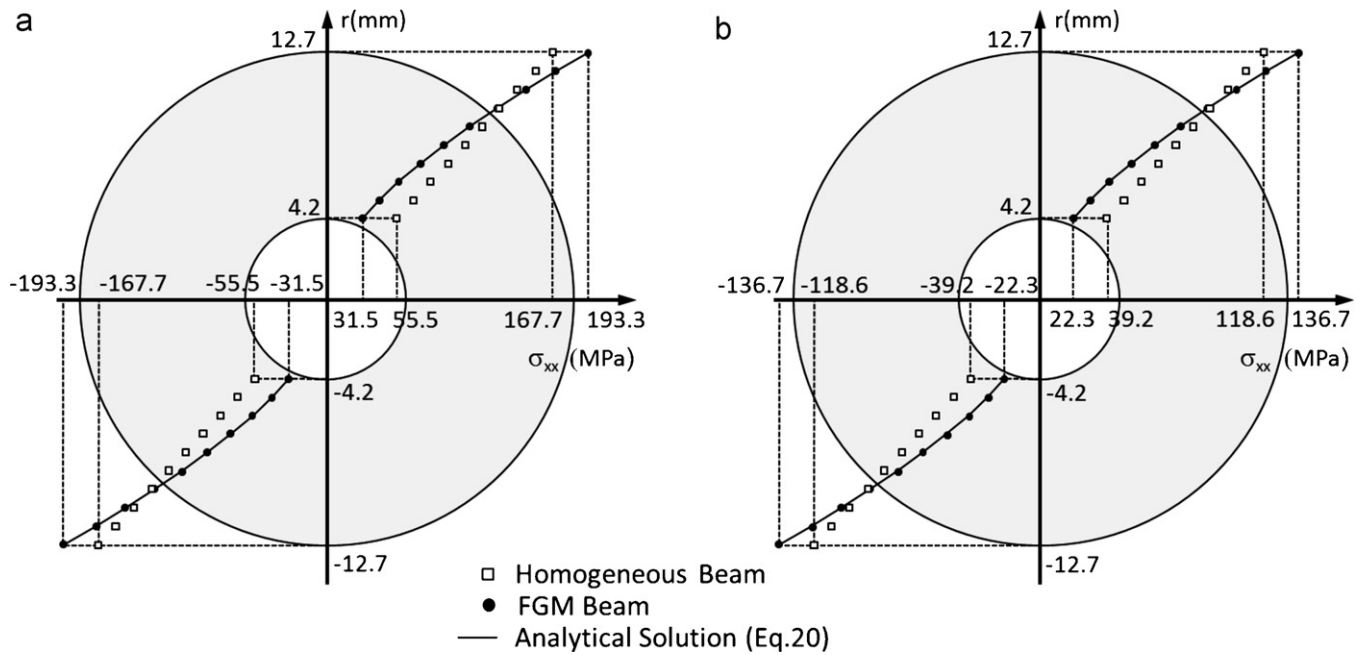
Fig. 10. Normal stresses at: (a) vertical cross-section cut and (b) 45° cross-section cut ($M = 0.6M^*$, $E(r) = 404(r/r_e)^{0.64}$GPa).
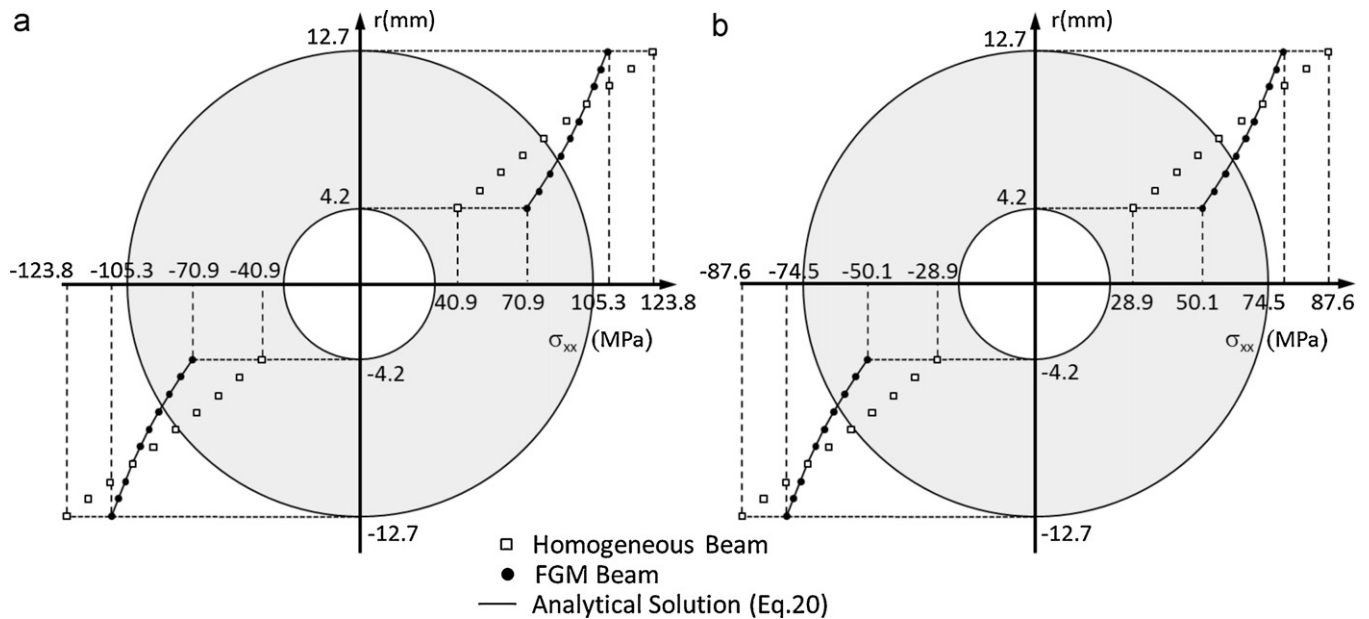
Fig. 11. Normal Stresses at: (a) Vertical Cross-Section Cut and (b) 45° Cross-Section Cut ($M = 0.6\,M^*$, $E(r) = 220\left(r/r_e\right)^{-0.64}$ GPa).

Fig. 10a and b presents normal stress distributions, furnished by the numerical analysis for FGM beam and by Eq. (20), along the beam for two different cross-section cuts: at a vertical cross-section and at 45° apart from this position, respectively. A very good agreement between these distributions is observed. Also, these results are compared to stresses in a homogenous beam cross-section having the same equivalent bending rigidity. For this particular loading, these plots show stress redistributions for the FGM material with 15% increase in the longitudinal stress maximum value and 43% decrease in its minimum value, as compared to linear distributions shown in the homogeneous material beam.

The obtained stress pattern distributions, which are dependent on the material Young's modulus through the pipe beam thickness, are changed if, for instance, the same large displacement beam analysis is carried out but with FGM cross section having TiC at the internal radius and Ni_3Al at external radius. In this case $E(r) = 220(r/r_e)^{-0.64}$ and the resulting stresses are as in Fig. 11a and b. In contrast to the obtained numerical results shown in Fig. 10a and b, new stress distributions, as compared to homogeneous beam results, reduce maximum stress values and increase the minimum ones.

5. Concluding remarks and extensions

This paper addresses a geometrically nonlinear analysis of functionally graded beams using a tailored Lagrangian formulation by means of a Total formulation. The effect of material gradation was incorporated in the formulation considering the beam ele-

ment effective cross-section rigidities associated to axial, shear and flexural deformation kinematics, all obtained in closed form from integration of the actual property variation through the thickness. Two numerical examples present a redistribution of stresses in the cross-section of functionally graded beams as compared to analytical solutions and to homogeneous beams. As shown in the examples, stress and displacement comparisons were considered. In the large displacement analysis, however, it was noticed that the beam of graded material presented a substantial difference in stress distributions as compared to the homogeneous one having the same equivalent cross-section rigidity.

The nonlinear techniques developed in this paper may be applicable to extend the existing body of work on linear formulations for functionally graded beams to the geometric nonlinear range. For instance, Silva et al. (2006) modeled bamboo as a linear functionally graded material. However, slender structures such as bamboo may exhibit second order behavior, which could be captured by the present geometrically nonlinear formulation.

We expect that this work will contribute to connect research with actual industrial applications. For instance, it is a first step towards development of functionally graded riser pipelines and pressure vessels, which may have promising applications in the petroleum industry (Rasmussen, 2008; Ilstad et al., 2006; Tutuncu, 2007). In this respect, future work includes extension of the present formulation to three-dimension analyses of FGM risers and considerations of dynamic loading conditions.

Acknowledgements

References

Almeida, S.R.M., Paulino, G.H., Silva, E.C.N., 2010. Layout and material gradation in topology optimization of functionally graded structures: a global–local approach. Structural and Multidisciplinary Optimization 42, 855–868.

Chakraborty, A., Gopalakrishnan, S., Reddy, J.N., 2003. A new beam finite element for the analysis of functionally graded materials. International Journal for Numerical Methods in Engineering 45, 519–539.

Chen, Y., Struble, L.J., Paulino, G.H., 2008. Using rheology to achieve co-extrusion of cement-based materials with graded cellular structures. International Journal of Applied Ceramic Technology 5[5], 513–521.

Choi, H.J., Paulino, G.H., 2010. Interfacial cracking in a graded coating/substrate system loaded by a frictional sliding flat punch. Proceedings of the Royal Society A 466, 853–880.

Dave, E.V., Paulino, G.H., Buttlar, W.G., 2011. Viscoelastic functionally graded finite-element method using correspondence principle. ASCE-Journal of Materials in Civil Engineering 23 (1), 39–48.

Ilstad, H., Naes, H.A., Endal, G., 2006. Strengthening Effect from Steel Pipe Cladding in Pure Bending. OMAE, Hamburg, Germany, paper 92524.

Kim, J.H., Paulino, G.H., 2002. Finite element evaluation of mixed mode stress intensity factors in functionally graded materials. International Journal for Numerical Methods in Engineering 53, 1903–1935.

Lages, E.N., Paulino, G.H., Menezes, I.F.M., Silva, R.R., 1999. Nonlinear finite element analysis using an object-oriented philosophy – application to beam elements and to the Cosserat continuum. Engineering with Computers 15, 73–89.

Miyamoto, Y., Kaysser, W.A., Rabin, B.H., Kawasaki, A., 1999. Functionally Graded Materials: Design, Processing and Applications. Springer, 352 pp.

Ng, T.Y., Lam, K.Y., Liew, K.M., 2000. Effects of FGM materials on the parametric resonance of plate structures. Computer Methods in Applied Mechanics and Engineering 190 (8–10), 953–962.

Pacoste, C., Eriksson, A., 1997. Beam elements in instability problems. Computer Methods in Applied Mechanics and Engineering 144, 163–197.

Paulino, G.H., Yin, H.M., Sun, L.Z., 2006. Micromechanics-based interfacial debonding model for damage of functionally graded materials with particle interactions. International Journal of Damage Mechanics.

Paulino, G.H., Sutradhar, A., 2006. The simple boundary element method for multiple cracks in functionally graded media governed by potential theory: a three-dimensional Galerkin approach. International Journal for Numerical Methods in Engineering 65, 2007–2034.

Paulino, G.H., Silva, E.C.N., Le, C.H., 2009. Optimal design of periodic functionally graded composites with prescribed properties. Structural and Multidisciplinary Optimization 38, 469–489.

Reddy, J.N., 1997. On locking-free shear deformable beam finite elements. Computer Methods in Applied Mechanics and Engineering 149, 113–132.

Rasmussen, K., 2008. JIP Lined and Clad Pipelines, Phase 2 – Installation and Operation, Local Buckling, DNV Report N°2007-3075, Revision 01.

Reddy, J.N., Cheng, Z.Q., 2001. Three-dimensional solutions of smart functionally graded plates. Journal of Applied Mechanics 68, 234–241.

Silva, E.C.N., Walters, M.C., Paulino, G.H., 2006. Modeling bamboo as a functionally graded material: lessons for the analysis of affordable materials. Journal of Materials Science 41, 6991–7004.

Shen, B., Hubler, M., Paulino, G.H., Struble, L.J., 2008. Functionally-graded fiber-reinforced cement composite: processing, microstructure, and properties. Cement & Concrete Composites 30, 663–673.

Suresh, S., Mortensen, A., Needleman, A., 1993. Fundamentals of Metal-Matrix Composites. Butterworth-Heinemann Publ, 400 pp.

Suresh, S., Mortensen, A., 1998. Fundamentals of Functionally Graded Materials. Maney Matls. Sci. Publ, 165 pp.

Tutuncu, N., 2007. Stresses in thick-walled FGM cylinders with exponentially varying properties. Engineering Structures 29, 2032–2035.

Yin, H.M., Sun, L.Z., Paulino, G.H., 2004. Micromechanics-based elastic model for functionally graded materials with particle interactions. Acta Materialia 52 (12), 3535–3543.

Zhang, Z., Paulino, G.H., 2007. Wave propagation and dynamic analysis of smoothly graded heterogeneous continua using graded finite elements. International Journal for Numerical Methods in Engineering 44, 3601–3626.